

Structures, Electronics, and Reactivity of Strained Phosphazane Cages: A Combined Experimental and Computational Study

Torsten Roth,[†] Vladislav Vasilenko,[†] Hubert Wadepohl,[†] Dominic S. Wright,^{*,‡} and Lutz H. Gade^{*,†}[†]Anorganisch-Chemisches Institut, Universität Heidelberg, Im Neuenheimer Feld 270, 69120 Heidelberg, Germany[‡]Chemistry Department, Cambridge University, Lensfield Road, Cambridge, CB2 1EW, U.K.

S Supporting Information

ABSTRACT: A series of formamidine-bridged P₂N₂ cages have been prepared. Upon deprotonation, these compounds serve as valuable precursors to hybrid N-heterocyclic carbene ligands, whereas direct metalation gives rearranged dimetallic complexes as a result of cleavage of the formamidine bridge. The latter metal complexes contain an intact cyclophosphazane moiety that coordinates two distinct metal centers in a monodentate and a chelating fashion. A computational study has been carried out to elucidate the bonding within the P₂N₂ framework as well as the reactivity patterns. Natural bond orbital analysis indicates that the cage motif is poorly described by localized Lewis structures and that negative hyperconjugation effects govern the stability of the bicyclic framework. The donor capacity of the cyclophosphazane unit was assessed by inspection of the frontier molecular orbitals, highlighting the fact that π -back-donation from the metal fragments is crucial for effective metal–ligand binding.

INTRODUCTION

Dimeric dichlorocyclophosph(III)azanes, [CIP(μ -NR)]₂, are versatile precursor materials for the preparation of a diverse range of cyclic and acyclic P,N-containing compounds.¹ A key feature of the chemistry of their P₂N₂ rings is the syn orientation of the exocyclic Cl substituents and the resulting C₂ rotational axis that is frequently retained in the solid and solution states. A major influence on the relative stability of the cis and trans isomers is the steric bulk of the acyclic R groups within the P₂N₂ motif. A widely used approach to constrain the cis geometry relies on the introduction of a rigid linker unit, which bridges one face of the P₂N₂ plane, by nucleophilic substitution of the Cl atoms.^{2,3} Such linkers have been based on diol or diamino groups or may contain further heteroatoms or metal centers (A and B in Figure 1).⁴

Typically, the linking unit comprises at least three atoms, although recent work by Schulz and co-workers established the formation of strained P,N-cage compounds (C) via intermediary phosphorus biradicaloids.⁵ Notably, the rearrangement of strained P₂N₂ cages may be exploited to access architecturally novel and diverse heterocyclic frameworks (D and E).⁶

Recently, we reported the preparation and crystallographic characterization of a hybrid cyclophosphazane–formamidinium salt (F) and its subsequent deprotonation and metalation (Scheme 1).⁷ In this way, a variety of structurally unique N-heterocyclic carbene (NHC) metal complexes comprising an intact bicyclic P,N-framework were accessed via the sequential introduction of different metal fragments.

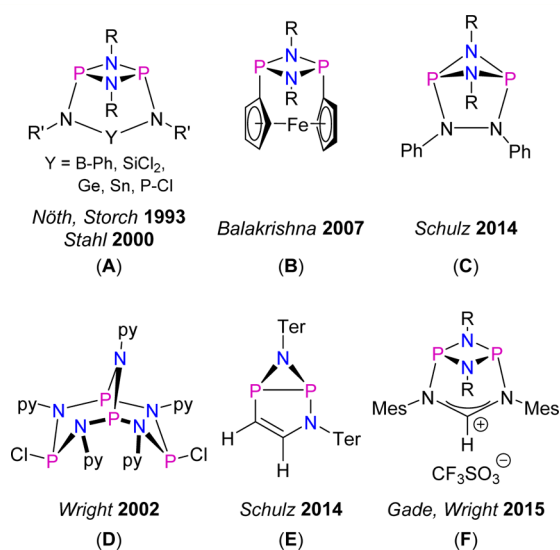
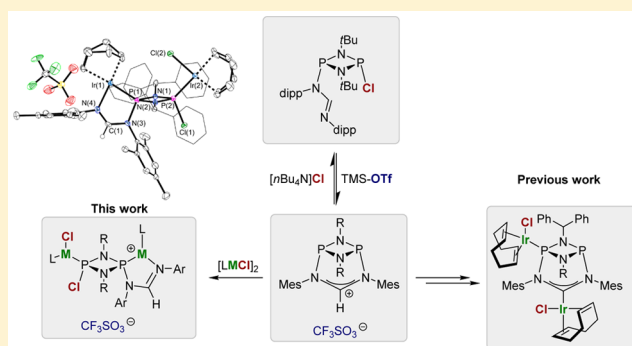


Figure 1. Selected P₂N₂ rings and related frameworks.

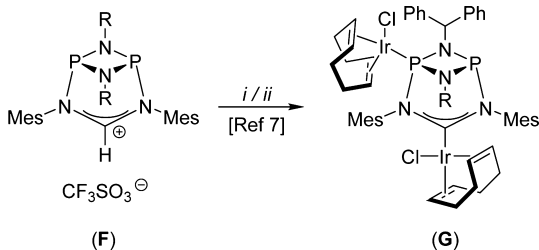
Here, we report the synthesis of a series of sterically and electronically diverse cationic cages of type F, a systematic investigation of their properties, and their coordination to late-transition-metal fragments. Such coordination is accompanied by cage opening at the formamidine bridge and contrasts with

Received: June 10, 2015

Published: July 16, 2015



Scheme 1. Deprotonation/Metalation Sequence of Cationic P_2N_2 Cages Leading to NHC Metal Complexes^a



^aReaction conditions: (i) KHMDS, toluene, room temperature; (ii) $[\text{Ir(cod)Cl}]_2$, toluene, room temperature.

retention of the cage structure in the carbene complex **G**. The observed reactivity motivated a computational study, and the bonding situation encountered was analyzed by means of natural bond orbital (NBO) theory.

RESULTS AND DISCUSSION

Synthesis and Structural Characterization of Cationic Cyclophosphazane Cages. We initially focused on the stepwise formation of the desired cationic cage compounds, using the dichlorocyclophosph(III)azane **1a**, the formamidine **2a**, and an excess of triethylamine to produce the unsymmetrically substituted P_2N_2 species **4a** (Scheme 2, top). The latter compound displays two doublet signals in the $^{31}\text{P}\{^1\text{H}\}$ NMR spectrum ($\delta_{\text{P}1} = 188.42$ ppm; $\delta_{\text{P}2} = 130.64$ ppm; $J_{\text{PP}} = 38.6$ Hz) and was structurally characterized by X-ray diffraction (Figure 2).

Although condensation of **1a** and **2a** selectively yielded the monosubstituted cyclophosphazane, the cationic product (**5a**) of the reaction of **4a** with $\text{Me}_3\text{Si-OTf}$ as the chloride scavenger degraded in solution.⁸ For this reason, more sterically shielding and electron-rich formamidines were chosen to stabilize the cationic frameworks. From a practical point of view, a

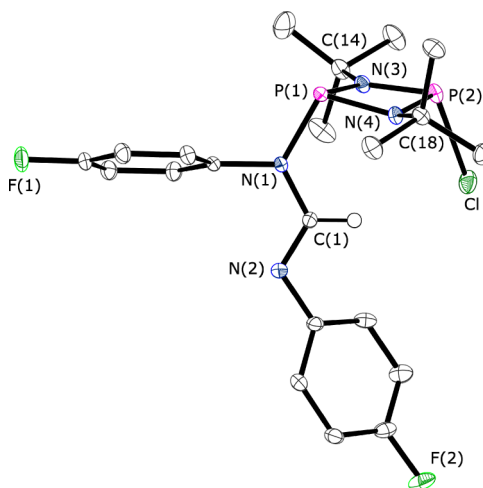


Figure 2. Molecular structure of **4a**. Thermal ellipsoids are set at the 50% probability level. H atoms have been omitted for clarity. Selected bond lengths [Å] and angles [deg]: P(1)–N(1) 1.7221(12), P(1)–N(3) 1.7296(13), N(1)–C(1) 1.3911(17), N(2)–C(1) 1.2737(17); N(1)–P(1)–P(2) 116.04(4), N(3)–P(1)–N(4) 79.96(5), N(2)–C(1)–N(1) 122.75(12).

generalized one-pot process starting from dichlorocyclophosph(III)azanes **1a–1d** and using the corresponding silyl-protected formamidines **3a–3d** proved to be the most efficient route to the target cages **5a–5h** (Scheme 2), giving the products in moderate to high yields (40–90%). Single crystals suitable for X-ray diffraction were obtained for **5b–5g**, and their solid state structures were determined. Selected structural parameters of all cationic cages are summarized in Table 1.

A comparison of the molecular structural parameters established for **5b–5g** supports the view of a rigid central cage framework that is only marginally influenced by the peripheral substituents. In contrast, the organic substituents on the P_2N_2 ring themselves are oriented in such a way as to avoid

Scheme 2. Preparation of Cationic Cyclophosph(III)azane Cages **5a–5h via a Two-Step Procedure (Top) or a One-Pot Protocol (Bottom)**

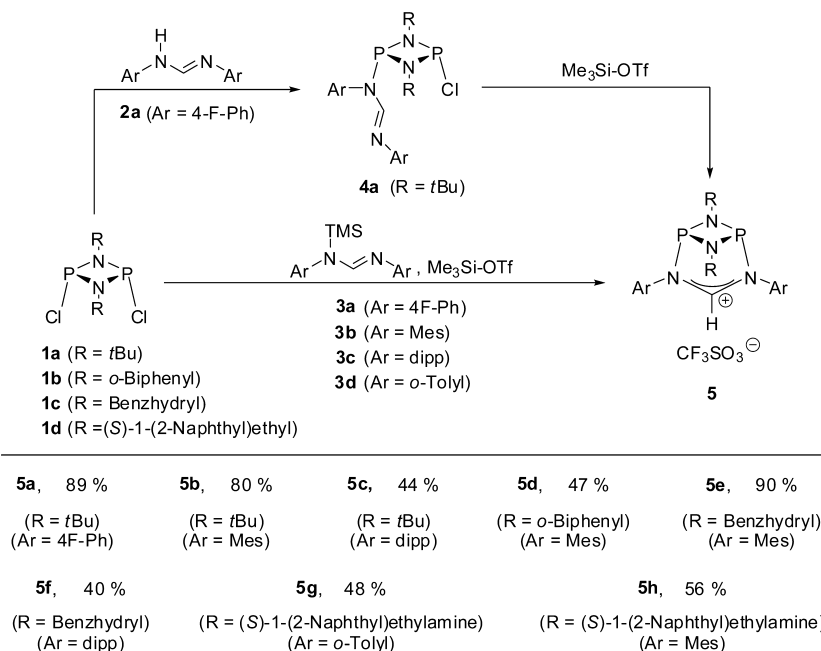
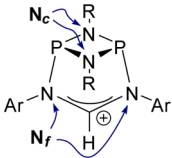


Table 1. Schematic Representation of the Cage Motif and Selected Structural Parameters of Compounds **5b–5g**


	<i>d</i> [Å]		angle [deg]	
	P–N _c ^a	P–N _f ^b	N–C–N	φ ^c
5b	1.7001(13)–1.7399(14)	1.7960(13), 1.8076(13)	122.6(1)	25.50(8)
5c	1.711(2)–1.732(2)	1.787(2), 1.797(2)	122.1(2)	23.5(1)
5d	1.6987(12)–1.7412(12)	1.8049(12), 1.8082(12)	122.6(1)	30.53(7)
5e^d	1.704(3)–1.716(3)	1.823(3), 1.837(3)	122.7(3)	31.4(1)
5f	1.706(3)–1.723(3)	1.821(3), 1.834(3)	124.3(4)	30.7(2)
5g	1.699(2)–1.724(2)	1.810(2), 1.815(2)	123.3(2)	31.2(1)

^aP–N_c denotes the range of P–N bond distances within the P₂N₂ ring. ^bP–N_f denotes the range of P–N bond distances between the P₂N₂ P atom and the formamidine N atom. ^cφ denotes the angle between the planes P–N(1)–P and P–N(2)–P. ^dTaken from ref 7.

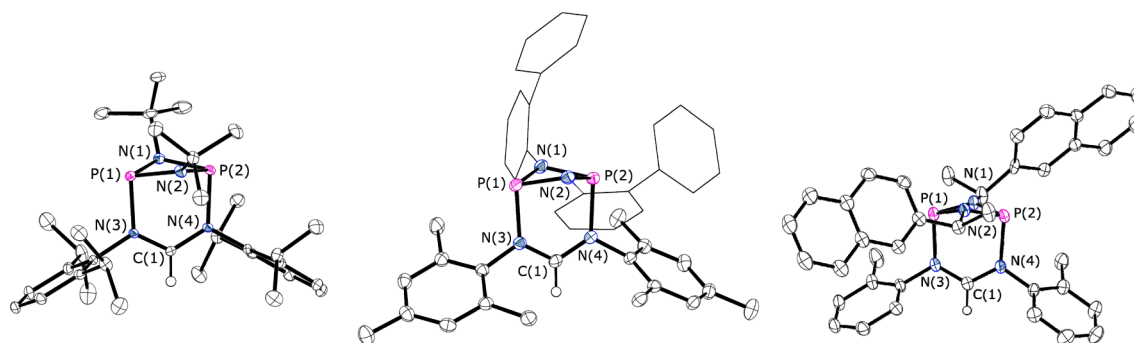
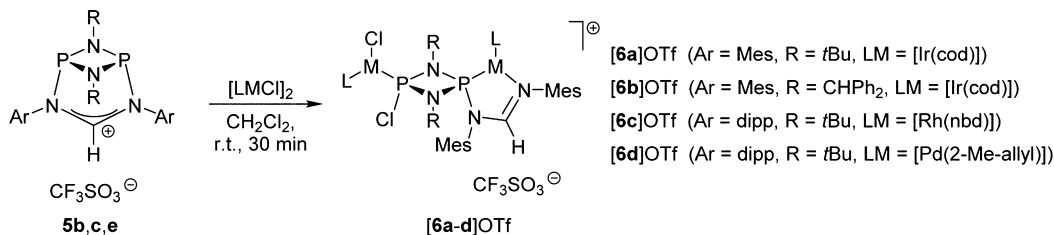


Figure 3. Solid-state structures of **5c** (left), **5d** (center), and **5g** (right). In the graphical representation of **5d**, the biphenyl units are drawn as wireframes. H atoms, except for C(1)–H, are omitted for clarity. The disorder in **5g** is not shown. For the molecular structures of **5b**, **5e**, and **5f**, see the SI.

Scheme 3. Ring-Opening Reaction of Cationic Cages Induced by Late-Transition-Metal Fragments



unfavorable steric interactions with the *o*-*i*Pr and Me substituents of the formamidine aryl groups (see Figure 3 and the Supporting Information, SI). A consistent feature of all of the cationic cages is the elongated bond between the P₂N₂ P atom and the formamidine unit (P–N_f = 1.79–1.83 Å) compared to the P–N distances within the P₂N₂ rings (P–N_c = 1.71–1.72 Å).⁹ In contrast, the *exo*-P–N bonds in unstrained bis(amino)cyclophosph(III)azanes are typically significantly shorter (1.68–1.71 Å).⁹ Moreover, the N–C–N angles at the formamidine bridges of the cationic cages **5b–5g** closely resemble those found in the protonated formamidine salts of **[2a + H][OTf]** and **[2b + H][OTf]**, indicating that any strain within the cage structures is mainly located at the P₂N₂ motif. This is supported by the significantly larger puckering angles (φ) of the P₂N₂ units found in compounds **5b–5g** [φ_{range} = 23.5(1)–31.4(1)°; Table 1] compared to those in the

corresponding dichlorocyclophosphazanes (e.g., **1a**, φ = 9.13°; **1b**, φ = 0.18°).¹⁰

Metalation of the Cationic P₂N₂ Cages. The deprotonation of compound **5e** yielding an NHC and its coordination chemistry with selected late-transition-metal fragments has been reported by us previously.⁷ In the current work, the focus is on the strained cationic cages themselves and their potential use as P donors for late-transition-metal complexes.¹¹ The coordination properties were assessed in reactions with iridium(I), rhodium(I), and palladium(II) precursors (giving the products **6a–6d**; Scheme 3). In all of the reactions investigated, clean formation of single products was observed after the reagents were mixed for 30 min at room temperature. Significantly, each of the products (**[6a–6c]OTf**) exhibited two doublet signals in the ³¹P NMR spectrum, indicating desymmetrization of the P₂N₂ unit.¹² The molecular structures of the three isostructural derivatives **[6a–6c]OTf** were

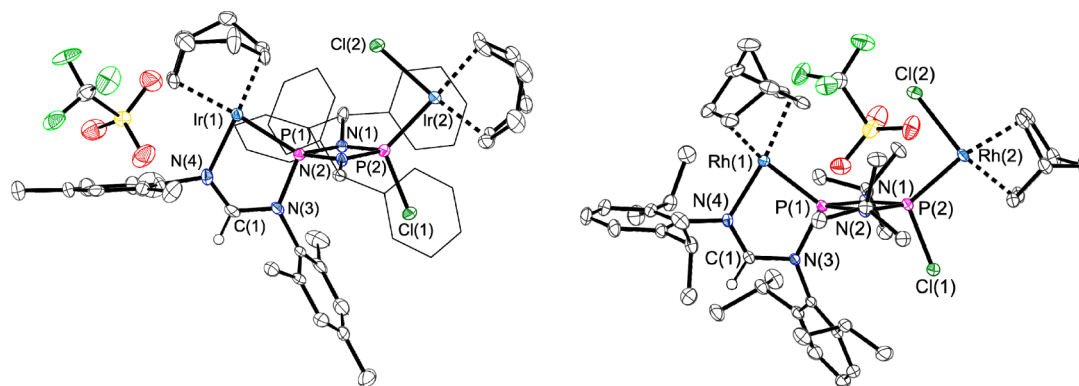


Figure 4. Molecular structure of $[6b]OTf$ (left) and $[6c]OTf$ (right). Thermal ellipsoids are set at the 50% probability level. H atoms, except for H(1), have been omitted for clarity. Phenyl rings of the benzhydryl substituents are drawn as wireframes. For selected bond lengths and angles, see Table 2.

Table 2. Selected Structural Parameters of Compounds $[6a-6c]OTf^a$

	<i>d</i> [Å]						angle [deg]
	M(1)–P(1)	M(2)–P(2)	P–N _c ^b	P(1)–N(3)	C(1)–N(3)	C(1)–N(4)	N–C–N
6a	2.217(2)	2.215(2)	1.696	1.779(5)	1.370(8)	1.285(8)	123.5(5)
6b	2.232(1)	2.218(1)	1.710	1.764(3)	1.366(5)	1.301(5)	123.9(4)
6c	2.2131(4)	2.2096(4)	1.695	1.790(3)	1.372(2)	1.294(2)	123.6(1)

^aFor the atom labeling, see Figure 4. ^bP–N_c denotes the average P–N bond distances within the P₂N₂ ring.

established by X-ray diffraction and revealed monodentate coordination of one metal fragment to one of the P atoms of the opened cage and chelating κ^2 -P,N coordination of the second metal center (Figure 4 and SI). The five-membered PN₂CM metallacyclic fragments of $[6a-6c]OTf$ adopt essentially planar conformations and are arranged orthogonally to the intact P₂N₂-ring units. In addition, cis coordination of the terminal and chelated metal centers with respect to the P₂N₂ cores is also observed. The M–C (cod/nbd) bonds that are located trans to the P atoms are slightly longer than the M–C bonds that are trans to chloride ligands, suggesting a significant trans influence of the P₂N₂–P unit compared to the chloride ligand. The M–P bond lengths are, however, all within the expected range of 2.21–2.23 Å, as are the metal–imine bonds (ca. 2.07 Å).¹³ The differing bond lengths within the N–C–N unit (mean 1.29 vs 1.37 Å within $[6a-6c]OTf$) may indicate little or no delocalization in contrast to the cationic cages.

A variable-temperature (VT) ³¹P NMR spectroscopic study of the palladium complex $[6d]OTf$ revealed dynamic behavior in solution (Figure 5). At low temperatures (–40 °C), the resonances of a 1:1 mixture of prone and supine isomers of $[6d]OTf$ (depending on the relative orientation of the two η^3 -methallyl ligands) were observed, while at elevated temperatures, a new set of signals emerged.¹⁴ This second species is interpreted as resulting from the reversible decooordination of a $[Pd(2-Me-allyl)Cl]$ fragment from the palladium(II) complex $[6d]OTf$, giving the mononuclear complex $[6d-mono]OTf$ (Scheme 4).¹⁵ The reaction enthalpy for decooordination ($\Delta H = 42 \text{ kJ mol}^{-1}$) was found to be similar to that previously reported for the analogous process in the related NHC cyclophosphazane iridium complex shown in Scheme 6.⁷

The cage-opening reaction seen in the formation of the metal complexes **6a–6d** (Scheme 3) can be regarded as occurring by chloride-induced ring opening and subsequent metal coordination.¹⁶ This view is supported by the finding that the cationic cage **5a** readily reacts with a stoichiometric amount of $[nBu_4N]$

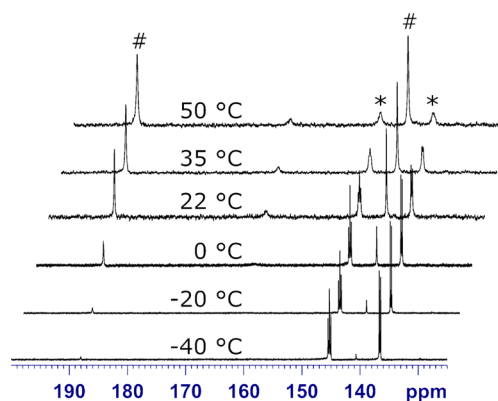
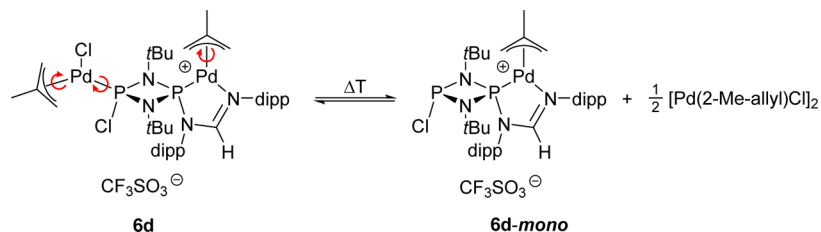


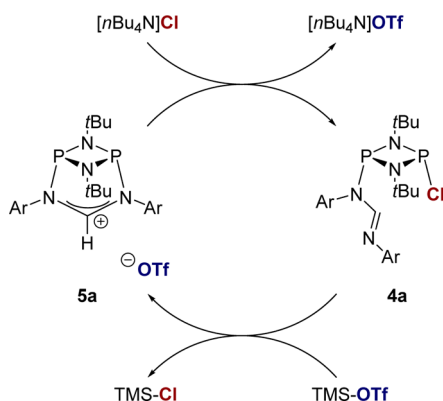
Figure 5. VT ³¹P NMR study of $[6d]OTf$. Signals marked by asterisks correspond to the dimetallic complex **6d**; the hashtag denotes the resonances corresponding to the monometallic complex $[6d-mono]OTf$.

Cl as a chloride source to form the corresponding ring-opened product **4a** (Scheme 5). In this context, the (reverse) ring-closing reaction of species like **4a** using Me₃Si-OTf can be regarded as part of an anion-dependent equilibrium (Scheme 5). Notably, a similar ring-opening reaction to **5a** is *not* observed when the cationic cage was deprotonated prior to metalation to give the corresponding carbene ligand.⁷ This contrasting reactivity (Scheme 6) indicated that the stability of the molecular cages reported in this work is governed by subtle electronic effects within the hybrid P₂N₂ framework, a feature that is explored using density functional theory (DFT) calculations later in the current work.

Computational Studies. In order to probe the reasons for the differences in reactivity between the phosphazane cations and the carbenes, DFT calculations were performed on a model cation (type I), free carbene (type II), and dimetallic iridium(I) complex (type III) (Figure 6). Notably, representatives of all of

Scheme 4. Reversible Coordination/Decoordination of $[\text{Pd}(2\text{-Me-ally})\text{Cl}]_2$ to the Palladium Complex $[\mathbf{6d}\text{-mono}]\text{OTf}^a$ 

^aIn solution, diastereomers of $[\mathbf{6d}]\text{OTf}$ are accessible by rotation around the highlighted bonds.

Scheme 5. Chloride-Induced Ring-Opening and Ring-Closing Reactions of the Cationic Cage $\mathbf{5a}$ ($\text{Ar} = 4\text{-F-Ph}$)

these species have been characterized previously by us or reported in this study, and there is thus a range of crystallographic data available for comparison with computed structures.

All computations were performed on simplified model systems (**M1–M3** in Figure 7), where substituents on the cage frameworks were replaced by methyl groups and the ligand set on Ir^{I} consisted of two π -bonded ethylene ligands and a chloride. During the course of the structural studies described above, we had found that the bicyclic core motif is only negligibly perturbed by the N substituents, rendering this simplification a legitimate approximation (see Table 1). Selected computed geometrical parameters as well as highest occupied molecular orbital (HOMO)/lowest unoccupied molecular orbital (LUMO) and promotion energies are presented in Table 3. Initial computational studies employing the standard B3LYP functional and 6-311++G** basis set gave poor agreement with experimentally determined molecular geometries, even when the full structures were modeled. In

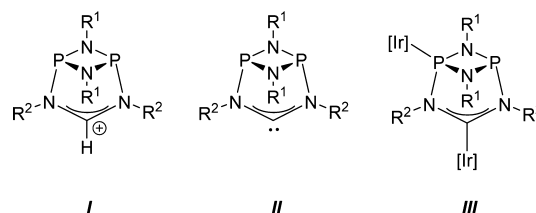


Figure 6. Structural types explored using model DFT calculations ($[\text{Ir}]$ is an organometallic iridium(I) fragment, e.g., **G**; Scheme 1).

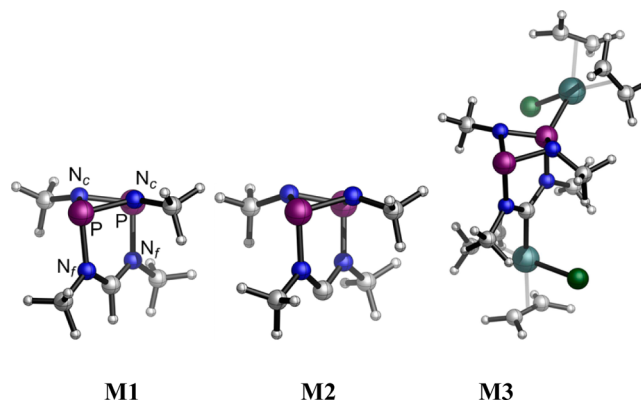
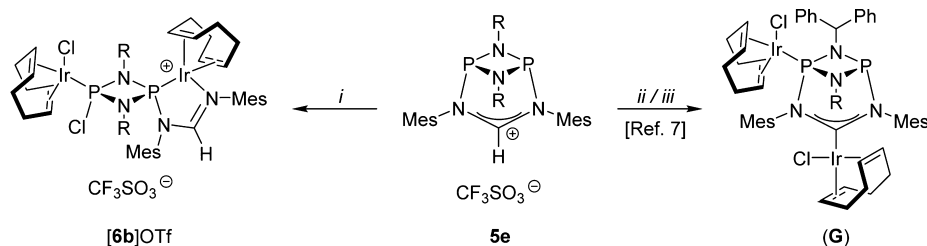


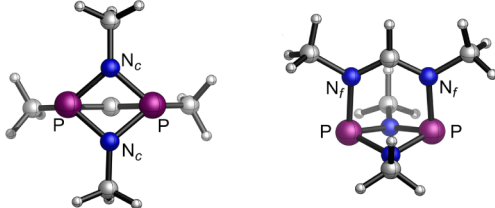
Figure 7. Molecular structures of models **M1–M3** at the PBE0-D/def2-TZVP level of theory. From left to right: **M1** is the cationic cage, **M2** the carbene, and **M3** the iridium(I) dimetallic complex. Color code: turquoise, Ir; dark green, Cl; purple, P; blue, N; gray, C; white, H.

particular, the most significant deviations were observed for the P–N_f bond to the formamidine bridge, which was computed to be generally more than 0.05 Å longer than that found in crystal structure analyses. In order to ensure that the computed geometries were accurate, a screening of basis sets and functionals was performed, and the combination of the

Scheme 6. Complementary Reactivity of Cationic P_2N_2 Cages in the Presence of Chloride-Containing Metal Precursors: (Left) Ring-Opening Reaction; (Right) Deprotonation and Metalation^a

^aReaction conditions: (i) $[\text{Ir}(\text{cod})\text{Cl}]_2$, CH_2Cl_2 , room temperature; (ii) KHMDS, toluene, room temperature; (iii) $[\text{Ir}(\text{cod})\text{Cl}]_2$, toluene, room temperature.

Table 3. Core Structure of the Model Systems and Selected Calculated Metric Parameters of Models **M1**–**M3** at the PBE0-D/def2-TZVP Level of Theory (Top) and Kohn–Sham HOMO/LUMO Energies and Gaps (Bottom)

			
bond/angle	<i>d</i> (Å)/ α (deg)		
	M1	M2	M3
N _f –P	1.81	1.76	1.75, ^a 1.72 ^b
N _c –P	1.71	1.73	1.71, 1.73 ^a
			1.68, 1.71 ^b
N _f –C–N _f	123.7	114.9	117.2
orbital	<i>E</i> / ΔE (eV)		
	M1	M2	M3
HOMO	–11.25	–5.39	–5.62
LUMO	–5.96	–1.42	–2.26
gap	5.29	3.97	3.37

^aBond lengths for the noncoordinated P. ^bBond lengths for the coordinated P.

dispersion-corrected PBE0 functional and def2-TZVP basis set was found to give the best results (for details, see the Experimental Section and SI).

A comparison of theoretical models **M1**–**M3** (Figure 7) with the experimentally determined structures (see Table 1) reveals close agreement with respect to the P₂N₂ units (Table 3). A noticeable contraction of the P–N_f bond length is seen upon going from the cation (**M1**, 1.81 Å) to the carbene (**M2**, 1.76 Å) and to the dimetallic complex (**M3**, 1.72 and 1.75 Å for the Ir-coordinated and uncoordinated P atoms, respectively). This trend is in excellent agreement with the parameters found in the experimental structures of the cations (range 1.79–1.83 Å; Table 1) and in the previously reported iridium(I) dimetallic complex **G** [1.756(3) and 1.760(3) Å; Scheme 1].^{7,17}

In order to obtain a qualitative understanding of the underlying bonding in these species and the changes that accompany metal deprotonation and metal coordination, we analyzed the Kohn–Sham frontier molecular orbitals (FMOs). For a graphical representation of selected FMOs for **M1**–**M3**,

see Figure 8 and the SI. While the FMOs share several common features, a few significant differences can be found. The Kohn–Sham HOMO of the carbene model **M2** is mainly located along the P–N_f bonds to the formamidine bridge, with additional contributions from the lone pairs of N_c and a large coefficient for the carbene lone pair. The HOMO of **M2** is therefore perfectly suitable for σ coordination to a metal fragment at the P and carbene centers. In contrast, the HOMO of the cationic cage **M1** is located around the P–N_c bonds of the P₂N₂ ring, with the P lobes being much closer to the P₂N₂ plane.¹⁸ All LUMOs of **M1**–**M3** were found to have π symmetry.

The composition, symmetry, and relative energies of the FMOs as well as their ordering have profound implications for the bonding of metals to the cation **M1** and the carbene **M2**. Given the FMOs of the free carbene **M2**, σ donation via the carbene center should lead to weaker, longer P–N_f bonds by depletion of the electron density from the HOMO. This is in line with the particularly long P–N_f bonds of the cationic cage **M1**. In contrast, the structures of the free carbene **M2** and the iridium complex **M3** are almost identical with respect to the P–N_f bond length. In part, this difference between **M1** and **M2** and **M3** can be attributed to the lower Lewis acidity of the neutral iridium fragment compared to a proton. Additionally, π -back-donation into the LUMO of **M2** can occur for electron-rich d metals like iridium, thus reinforcing the P–N_f bonds. Bonding of metal fragments via the P atoms can be explained in a similar fashion. Following the analysis outlined above, σ coordination of the P atom to a metal should, in principle, produce weaker P–N_f bonds. In practice, however, complexes containing P-coordinated metals feature much shorter P–N_f bonds, indicating that σ coordination merely plays a secondary role compared to π -back-bonding. In addition to its donation properties, the cage **M2** is also an excellent π acceptor featuring a low-lying LUMO. Accordingly, donation of electron density from filled metal d orbitals into the LUMO accounts for a major part of the P–M bond. This is in agreement with the results reported by Frenking et al., who found that bonding of weak donor ligands such as PCl₃ to transition metals, electrostatic effects aside, mainly consists of π -back-bonding.¹⁹ Most importantly, interactions of this type produce stronger P–N_f bonds by donation of electron density into the LUMO, that is, bonding with respect to the P–N_f bond.

To explore the bonding situation in the cages further, all model compounds were investigated by means of NBO analysis. Analysis of the models **M1**–**M3** shows that these cages are only poorly described by localized bonding alone. This delocalization extends beyond that expected over the

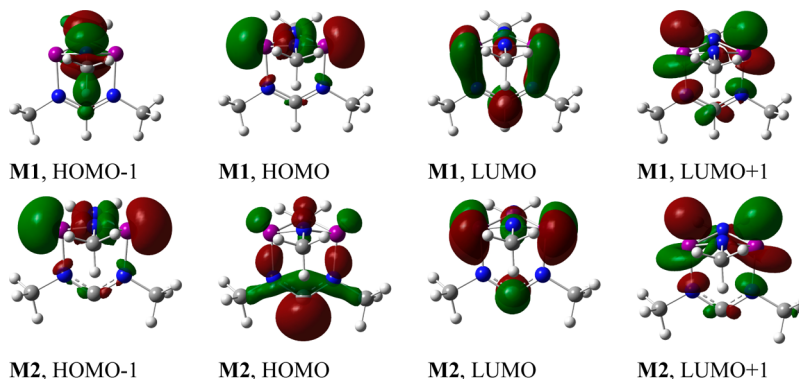


Figure 8. Kohn–Sham FMOs of models **M1** and **M2** computed at the PBE0-D/def2-TZVP level of theory. An isovalue of 0.05 was used.

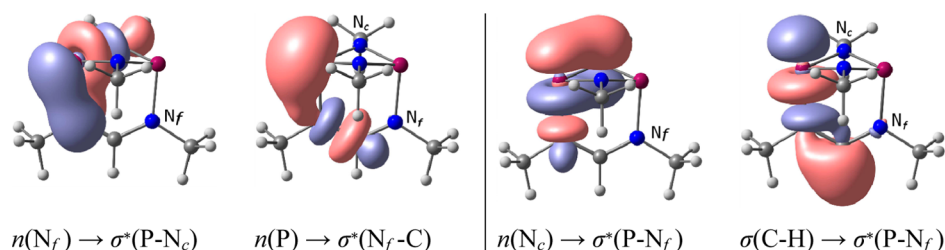


Figure 9. Stabilizing (left) and destabilizing (right) donor–acceptor contributions to the P–N_f bonds in the model cation **M1**.

formamidinium bridges of **M1**–**M3**. Owing to strongly delocalized bonding, small changes in the cage structures, e.g., protonation of the carbene center or metal coordination to the P centers, can have a dominant effect on the properties of the cage as a whole. An overview of the most prominent NBO interactions in **M1** is shown in Figure 9.

Two major types of interactions can be distinguished in the cages: (i) P–N_f destabilizing contributions and (ii) P–N_f stabilizing contributions (see Table 4). These are shown for

Table 4. Summary of Selected Donor–Acceptor Interactions in Models **M1**–**M3**^a

#	<i>E</i> (D→A) (kcal mol ^{−1})			
	$n(N_c) \rightarrow \sigma^*(P-N_f)$	$\sigma(C-X) \rightarrow \sigma^*(N_f-P)$	$n(N_f) \rightarrow \sigma^*(P-N_c)$	$n(P) \rightarrow \sigma^*(N_f-C)$
M1	41.0	10.1	7.6	10.5
M2	30.4	28.8	11.6	14.2
M3	36.4	19.2	10.8	14.3

^aIn the case of several analogous interactions, the total sum is provided. Stabilizations ΔE were determined as estimates calculated from second-order perturbation theory.

the cation **M1** in Figure 9. The relative strength of these interactions is critically dependent on the structure of the complex. Donation of electron density from the $n(N_c)$ lone pair into the $\sigma^*(P-N_f)$ orbital is particularly pronounced in the cationic cage compound **M1**, resulting in weakened P–N_f bonds (Figure 9, right). This is caused by a smaller energetic splitting between the donor and acceptor orbitals in the cationic model. Additional destabilization of this bond arises from donation of electron density from the (pre)carbenic center into the $\sigma^*(P-N_f)$ orbital. The extent of this interaction depends on the bonding partner of the carbene C atom and follows the order $n(C) > \sigma(C- Ir) > \sigma(C-H)$. Stabilization of the P–N_f bonds mainly occurs through donation of electron density from the N_f lone pairs into the $\sigma^*(P-N_c)$ orbital and from the P lone pairs into the $\sigma^*(N_f-C)$ orbitals (Figure 9, left). In line with the lability of the P–N_f bond in the cationic cage, these stabilizing interactions were found to play only a minor role in **M1**, overall leading to a significantly weaker attachment of the bridging formamidinium unit to the cyclophosphazane ring, compared to all other structures. For a summary of the most prominent donor–acceptor interactions, see Table 4.

The poor P– σ -bonding properties of cages are reflected in the hybridization of P lone pairs (Table 5) because coordination of a metal to the P atoms usually leads to significant polarization of the lone pair and thus to higher p character. Therefore, the donor ability of a phosphine is best assessed by comparing the p character observed upon coordination of the metal fragment (**M2** → **M3**).

Table 5. (Lone-Pair) Hybridization for Model Compounds **M1**–**M3**

#	hybridization (sp ⁿ)			
	N _f	N _c	P	C
M1	p ¹	sp ^{9.28}	sp ^{0.63}	sp ^{2.17}
M2	p ¹	sp ^{5.72}	sp ^{0.71}	sp ^{1.21}
M3	p ¹	sp ^{8.00}	sp ^{1.44^a}	sp ^{1.60}

^aCoordinated to iridium.

As has been shown by Frenking and co-workers, weak donors like PF₃ and PCl₃ have a very high s character in the free ligand (76% and 80%), which is substantially reduced upon coordination to transition metals, e.g., to 19% and 30% in chromium pentacarbonyl complexes [Cr(CO)₅PX₃].¹⁹ Similarly, deprotonation of the cationic cage **M1** decreases the s character only to a small extent (61% in **M1** vs 58% in **M2**), whereas coordination of iridium gives more directional bonds with 41% s character in **M3**. Remarkably, the p character of the metal-coordinated cage **M3** is even lower than that in complexes of the extremely weak donors PCl₃ and PF₃, thus underlining the extraordinarily low P– σ -donor strength of this class of compounds. These findings are in agreement with the results obtained from analysis of the FMOs, where the P₂N₂ backbone was identified as excellent π -acceptor and poor σ -donor units.

CONCLUSION

We have developed a general method for the preparation of bicyclic formamidinium-bridged cyclophosphazanes via either a two-step protocol or a one-pot procedure. The molecular structures of these compounds were established by X-ray structure analysis, corroborating a highly strained cage framework shielded by the peripheral substituents. Subsequent metalation of the cationic cages *without prior conversion to a carbene ligand* results in rearrangement of the phosphazane frameworks, as seen in the resulting dinuclear rhodium, iridium, and palladium complexes, in which cleavage of the formamidinium bridges had occurred. This reactivity pattern contrasts with that of the carbenes (derived from deprotonation of the cations), which coordinate transition-metal fragments without degradation of the phosphazane units.

Analysis of the Kohn–Sham FMOs and NBOs in model cation, carbene, and carbene–transition metal complexes highlights the important influence of delocalized bonding on their reactivities, stabilities, and coordination properties. In particular, calculations reveal that, like the P atoms of the derived carbene ligands, the P atoms of the cations have predominantly π -acceptor character and very low σ -donor character. These studies inform future work in this area by providing a potential basis for the ways in which the acceptor

and donor character of related main-group ligand systems might be tuned by structural changes.

EXPERIMENTAL SECTION

All manipulations were carried out under exclusion of air and moisture using standard Schlenk and glovebox techniques. As inert gas, Argon 5.0, purchased from Messer Group GmbH, was used after drying over Granusic phosphorpentoxide granulate. Solvents were dried over activated alumina columns using a solvent purification system (M. Braun SPS 800) or according to standard literature methods²⁰ and stored in glass ampules under an argon atmosphere. Degassed solvents were obtained by three successive freeze–pump–thaw cycles. Phosphorus trichloride was distilled prior to use, and triethylamine was degassed. NMR spectra were recorded on Bruker Avance (400, 500, and 600 MHz) instruments. Chemical shifts (δ) are reported in parts per million (ppm) and are referenced to residual proton solvent signals or carbon resonances.²¹ H_3PO_4 (^{31}P) and CCl_3F (^{19}F) were used as external standards. High-resolution mass spectrometry (MS) spectra were acquired on Bruker ApexQe hybrid 9.4 T FT-ICR (ESI) and JEOL JMS-700 magnetic sector (FAB, EI, and LIFDI) spectrometers at the mass spectrometry facility of the Institute of Organic Chemistry, University of Heidelberg. Elemental analyses were carried out in the Microanalysis Laboratory, Chemistry Department, University of Heidelberg, on a vario MICRO cube (Elementar). All chemicals were obtained from commercial suppliers and were used without further purification. The dichlorocyclophosphazanes **1a–1d**,³ formamides,²² and silylated formamides²³ were prepared following established procedures.

General Procedure for the One-Pot Preparation of Cationic Cyclophosphazane Cages **5a–5h.** To a solution of the dichlorocyclophosphazane **1** (1 equiv) in toluene was added a solution of the silylated formamidine **3** (1 equiv) in toluene dropwise at room temperature. The mixture was stirred for 1 h and then cooled to $-40\text{ }^\circ\text{C}$, and a cooled solution of TMS-OTf (1 equiv) in toluene (10 mL) was added dropwise. After the indicated time, the reaction mixture was filtered, and the residue was washed with toluene and dried in vacuo, affording product **5** as a colorless solid. For full analytical and spectroscopic characterization of **5a–5h**, see the SI.

Exemplary Data for **5c:** colorless solid, 44%. ^1H NMR (THF- d_8 , 600.13 MHz, 295 K): δ 8.47 (m, 1H, H-3), 7.58–7.53 (m, 2H, H-7), 7.48 (d, J = 7.8 Hz, 4H, H-6), 3.23 (sept, J = 6.8 Hz, 4H, H-8), 1.61 (s, 18H, H-2), 1.33 (d, J = 6.8 Hz, 12H, H-9), 1.30 (d, J = 6.8 Hz, 12H, H-9'). $^{13}\text{C}\{^1\text{H}\}$ NMR (THF- d_8 , 150.90 MHz, 295 K): δ 151.69 (s, C-3), 146.60 (s, C-5), 136.37 (d, J = 10.1 Hz, C-4), 131.96 (s, C-7), 126.56 (s, C-6), 58.29 (t, J = 8.8 Hz, C-1), 30.83 (t, J = 6.0 Hz, C-2), 30.29 (s, C-8), 25.28 (s, C-9), 25.18 (s, C-9'). $^{31}\text{P}\{^1\text{H}\}$ NMR (THF- d_8 , 242.94 MHz, 295 K): δ 248.73 (s). Elem. anal. Calcd for $\text{C}_{34}\text{H}_{53}\text{F}_3\text{N}_4\text{O}_3\text{P}_2\text{S}$: C, 56.97; H, 7.45; N, 7.82. Found: C, 56.90; H, 7.40; N, 7.83. MS [LIFDI(+)]. Calcd for $\text{C}_{33}\text{H}_{53}\text{N}_4\text{P}_2$: m/z 567.4. Found: m/z 567.1 ($[\text{M} - \text{OTf}]^+$). The spectroscopic data for the other cationic cyclophosphazanes as well as the atom labeling can be found in the SI.

General Procedure for the Preparation of Dimetallic Complexes **[6a–6d]OTf.** To a solution of **5** (100 mg, 1 equiv) in CH_2Cl_2 at room temperature was added a solution of $[\text{LMCl}]_2$ (1 equiv) in CH_2Cl_2 , and stirring was continued overnight. Then, the solvent was concentrated to a minimum, and the remaining solution was carefully layered with toluene and *n*-pentane. The mixture was kept at room temperature for ca. 1 week, then the supernatant was decanted, and the crystalline solid of **[6a–6d]OTf** was washed with *n*-pentane and dried in vacuo. The spectroscopic data for the dimetallic complexes **[6a–6d]OTf** can be found in the SI.

COMPUTATIONAL DETAILS

The computational software ORCA 3.0 was used for geometry optimizations and frequency calculations.²⁴ NBO analysis was performed by the NBO 6.0 package, as implemented in Gaussian 09, revision B.01.²⁵ All geometry optimizations of model compounds were carried out with Ahlrichs' def2-TZVP basis functions²⁶ and the

dispersion-corrected PBE0 functional,^{27,28} employing the RIJCOSX approximation, as implemented in the ORCA 3.0 software suite.²⁹ The absence of imaginary frequencies was confirmed by numerical frequency calculations.

ASSOCIATED CONTENT

Supporting Information

Methods and characterization data, details of the computational studies, optimized structures, and CIF files giving crystallographic data. The Supporting Information is available free of charge on the ACS Publications website at DOI: 10.1021/acs.inorgchem.5b01292.

AUTHOR INFORMATION

Corresponding Authors

*E-mail: dsw1000@cam.ac.uk.

*E-mail: lutz.gade@uni-heidelberg.de.

Notes

The authors declare no competing financial interest.

ACKNOWLEDGMENTS

We gratefully acknowledge the award of a Ph.D. grant to T.R. from Landesgraduiertenförderung (LGF Funding Program of the State Baden-Württemberg), the award of a national scholarship (Deutschlandstipendium) to V.V., the University of Heidelberg for generous funding, and the ERC-Advanced Investigator Grant to D.S.W. We are grateful to Sebastian Intorp and Clemens Blasius for experimental support.

REFERENCES

- (1) (a) He, G.; Shynkaruk, O.; Lui, M. W.; Rivard, E. *Chem. Rev.* **2014**, *114*, 7815. (b) Chivers, T.; Manners, I. *Inorganic Rings and Polymers of the p-Block Elements: From Fundamentals to Applications*; Royal Society of Chemistry: London, 2009. (c) Stahl, L. *Coord. Chem. Rev.* **2000**, *210*, 203–250. (d) Keat, R. *Inorganic Ring Systems; Topics in Current Chemistry*; Springer: Berlin, 1982; Vol. 102; Chapter 2, pp 89–116.
- (2) Keat, R.; Thompson, D. G. *Angew. Chem., Int. Ed. Engl.* **1977**, *16*, 797–798.
- (3) For more examples of bridging units, see the following. Unsymmetric: Kumaravel, S. S.; Krishnamurthy, S. S.; Cameron, T. S.; Linden, A. *Inorg. Chem.* **1988**, *27*, 4546–4550. Fluorinated: Kamil, W. A.; Bond, M. R.; Willett, R. D.; Shreeve, J. M. *Inorg. Chem.* **1987**, *26*, 2829–2833. Diaryloxide: Vijulatha, M.; Kumaraswamy, S.; Kumara Swamy, K. C.; Engelhardt, U. *Polyhedron* **1999**, *18*, 2557–2562. Chiral linkers: Chakravarty, M.; Kommana, P.; Swamy, K. C. K. *Chem. Commun.* **2005**, 5396–5398. Kumara Swamy, K. C.; Gangadhararao, G.; Srinivas, V.; Bhuvan Kumar, N. N.; Balaraman, E.; Chakravarty, M. *Inorg. Chim. Acta* **2011**, *372*, 374–382. Roth, T.; Wadeh, H.; Wright, D. S.; Gade, L. H. *Chem. - Eur. J.* **2013**, *19*, 13823–13837.
- (4) (a) Linti, G.; Nöth, H.; Schneider, E.; Storch, W. *Chem. Ber.* **1993**, *126*, 619–629. (b) Balakrishna, M. S.; Mague, J. T. *Organometallics* **2007**, *26*, 4677–4679. (c) Siddiqui, M. M.; Mobin, S. M.; Senkovska, I.; Kaskel, S.; Balakrishna, M. S. *Chem. Commun.* **2014**, *50*, 12273–12276.
- (5) (a) Hinz, A.; Kuzora, R.; Rosenthal, U.; Schulz, A.; Villinger, A. *Chem. - Eur. J.* **2014**, *20*, 14659–14673. (b) Hinz, A.; Schulz, A.; Villinger, A. *Chem. - Eur. J.* **2014**, *20*, 3913–3916.
- (6) (a) Bashall, A.; Doyle, E. L.; Garcia, F.; Lawson, G. T.; Linton, D. J.; Moncrieff, D.; McPartlin, M.; Woods, A. D.; Wright, D. S. *Chem. - Eur. J.* **2002**, *8*, 5723–5731. (b) Hinz, A.; Schulz, A.; Seidel, W. W.; Villinger, A. *Inorg. Chem.* **2014**, *53*, 11682–11690.
- (7) Roth, T.; Vasilenko, V.; Benson, C. G. M.; Wadeh, H.; Wright, D. S.; Gade, L. H. *Chem. Sci.* **2015**, *6*, 2506–2510.

- (8) Benhamou, L.; Chardon, E.; Lavigne, G.; Bellemin-Laponnaz, S.; César, V. *Chem. Rev.* **2011**, *111*, 2705–2733.
- (9) According to a search of CSD, version 5.36 (Nov 2014): Allen, F. H. *Acta Crystallogr., Sect. B: Struct. Sci.* **2002**, *58*, 380–388.
- (10) The solid-state structures of $[2a + H][OTf]$ and $[2b + H][OTf]$ were established by X-ray diffraction. For a representation, see the SI. The solid-state structure of the *tert*-butyl-substituted cyclophosphazane **1a** has been reported: Muir, K. W. *J. Chem. Soc., Dalton Trans.* **1975**, 259–262.
- (11) The coordination chemistry of P_2N_2 rings and late-transition-metal fragments has been explored thoroughly. For example, see: (a) Balakrishna, M. S.; Reddy, V. S.; Krishnamurthy, S. S.; Nixon, J. F.; Burckett St. Laurent, J. C. T. R. *Coord. Chem. Rev.* **1994**, *129*, 1–90. (b) Balakrishna, M. S. *J. Organomet. Chem.* **2010**, *695*, 925–936. (c) Krishnamurthy, S. S.; Reddy, V. S.; Chandrasekaran, A.; Nethaji, M. *Phosphorus, Sulfur Silicon Relat. Elem.* **1992**, *64*, 99–106. See also ref 3.
- (12) An additional splitting of the signals due to P–Rh coupling is observed for compound **6c** ($J_{PRh} = 283$ and 272 Hz).
- (13) The observed M–P and M–N bond lengths are comparable to related structurally characterized complexes. For example, see: Hilgraf, R.; Pfaltz, A. *Adv. Synth. Catal.* **2005**, *347*, 61–77.
- (14) The mechanism and thermodynamics of the interconversion of the two isomeric species of **6d** were not investigated because of the complexity of the system. For related studies on palladium(II) allyl complexes, see: (a) Pregosin, P. S.; Salzmann, R. *Coord. Chem. Rev.* **1996**, *155*, 35–68. (b) Kleimark, J.; Norrby, P.-O. In *Computational Insights into Palladium-Mediated Allylic Substitution Reactions*; Kazmaier, U., Ed.; Topics in Organometallic Chemistry 38; Springer: Berlin, 2012; pp 65–93. (c) Filipuzzi, S.; Pregosin, P. S.; Albinati, A.; Rizzato, S. *Organometallics* **2006**, *25*, 5955–5964. See also ref 7.
- (15) This is supported by (i) the ^{31}P NMR chemical shifts of the species emerging at elevated temperatures (at room temperature, δ 188.69 and 141.91) and (ii) the room temperature 1H and ^{13}C NMR spectra displaying signals corresponding to the uncoordinated allylpalladium(II) dimer.
- (16) Ring opening of the P_2N_2 unit was not observed herein. In contrast, previous studies by Burford and co-workers observed ring expansion of the central P_2N_2 motif induced by Lewis acids: (a) Burford, N.; Cameron, T. S.; Conroy, K. D.; Ellis, B.; Lumsden, M.; Macdonald, C. L. B.; McDonald, R.; Phillips, A. D.; Ragogna, P. J.; Schurko, R. W.; Walsh, D.; Wasylishen, R. E. *J. Am. Chem. Soc.* **2002**, *124*, 14012–14014. (b) Burford, N.; Conroy, K. D.; Landry, J. C.; Ragogna, P. J.; Ferguson, M. J.; McDonald, R. *Inorg. Chem.* **2004**, *43*, 8245–8251.
- (17) Buckling of the cyclophosphazane N substituents was found in both the crystal and fully calculated structures. Although this effect has been observed with phosphazanes before, the extent of buckling is extraordinary and previous relevant examples are limited to metal complexes where one of the phosphazane N atoms weakly coordinates to a metal fragment. For example, see: (a) Schranz, I.; Stahl, L. *Inorg. Chim. Acta* **2010**, *363*, 975–980. (b) Albahily, K.; Ahmed, Z.; Gambarotta, S.; Koc, E.; Duchateau, R.; Korobkov, I. *Organometallics* **2011**, *30* (21), 6022–6027. We suggest that this finding is the result of steric repulsion of the phosphazane and formamidine substituents.
- (18) It should be noted that the same type of orbital can also be found in the acyclic model **M1** and the free carbene **M3**, although in both cases, it is much lower in energy (HOMO–2 for **M1** and HOMO–1 for **M3**). Because of the positive charge, the orbital corresponding to the P–N $_i$ bond is much lower in energy than the HOMO (HOMO–2).
- (19) Frenking, G.; Wichmann, K.; Fröhlich, N.; Grobe, J.; Golla, W.; Van, D. L.; Krebs, B.; Läge, M. *Organometallics* **2002**, *21*, 2921–2930.
- (20) Armarego, W. L. F.; Chai, C. L. L. *Purification of Laboratory Chemicals*, 7th ed.; Butterworth-Heinemann: Oxford, U.K., 2012.
- (21) (a) Fulmer, G. R.; Miller, A. J. M.; Sherden, N. H.; Gottlieb, H. E.; Nudelman, A.; Stoltz, B. M.; Bercaw, J. E.; Goldberg, K. I. *Organometallics* **2010**, *29*, 2176–2179. (b) Gottlieb, H. E.; Kotlyar, V.; Nudelman, A. *J. Org. Chem.* **1997**, *62*, 7512–7515.
- (22) Kuhn, K. M.; Grubbs, R. H. *Org. Lett.* **2008**, *10*, 2075–2077.
- (23) Despagne-Ayoub, E.; Grubbs, R. H. *J. Am. Chem. Soc.* **2004**, *126*, 10198–10199.
- (24) Neese, F. *WIREs Comput. Mol. Sci.* **2012**, *2*, 73–78.
- (25) (a) Glendenning, E. D.; Badenhop, J. K.; Reed, A. E.; Carpenter, J. E.; Bohmann, J. A.; Morales, C. M.; Landis, C. R.; Weinhold, F. *NBO 6.0*; Theoretical Chemistry Institute, University of Wisconsin: Madison, WI, 2013. (b) Frisch, M. J.; et al. *Gaussian 09*, revision B.01; Gaussian Inc.: Wallingford, CT, 2009.
- (26) (a) Weigend, F.; Ahlrichs, R. *Phys. Chem. Chem. Phys.* **2005**, *7*, 3297–3305. (b) Weigend, F. *Phys. Chem. Chem. Phys.* **2006**, *8*, 1057–1065.
- (27) (a) Grimme, S.; Antony, J.; Ehrlich, S.; Krieg, H. *J. Chem. Phys.* **2010**, *132*, 154104. (b) Grimme, S.; Ehrlich, S.; Goerigk, L. *J. Comput. Chem.* **2011**, *32*, 1456–1465.
- (28) (a) Adamo, C.; Barone, V. *J. Chem. Phys.* **1999**, *110*, 6158–6170. (b) Ernzerhof, M.; Scuseria, G. E. *J. Chem. Phys.* **1999**, *110*, 5029.
- (29) (a) Izsak, R.; Neese, F. *J. Chem. Phys.* **2011**, *135*, 144105. (b) Neese, F. *J. Comput. Chem.* **2003**, *24*, 1740–1747.